Journal of Biomechanics 44 (2011) 1361–1366

Contents lists available at ScienceDirect

Journal of Biomechanics

journal homepage: www.elsevier.com/locate/jbiomech
www.JBiomech.com

Rupture of plasma membrane under tension

Samuel Chun Wei Tan, Tianyi Yang, Yingxue Gong [1], Kin Liao *

Division of Bioengineering, School of Chemical and Biomedical Engineering, Nanyang Technological University, Singapore 637457, Singapore

ARTICLE INFO

Article history:
Accepted 2 January 2011

Keywords:
Plasma membrane
Rupture
Tensile strength
Weibull distribution

ABSTRACT

We present a study on the rupture behavior of single NIH 3T3 mouse fibroblasts under tension using micropipette aspiration. Membrane rupture was characterized by breaking and formation of an enclosed membrane linked to a tether at the cell apex. Three different rupture modes, namely: single break, initial multiple breaks, and continuous multiple breaks, were observed under similar loading condition. The measured mean tensile strengths of plasma membrane were 3.83 ± 1.94 and 3.98 ± 1.54 mN/m for control cells and cells labeled with TubulinTracker™, respectively. The tensile strength data was described by Weibull distribution. For the control cells, the Weibull modulus and characteristic strength were 1.86 and 4.40 mN/m, respectively; for cells labeled with TubulinTracker™, the Weibull modulus and characteristic strength were 2.68 and 4.48 mN/m, respectively. Based on the experimental data, the estimated average transmembrane proteins–lipid cleavage strength was 2.64 ± 0.64 mN/m. From the random sampling of volume ratio of transmembrane proteins in cell membrane, we concluded that the Weibull characteristic of plasma membrane strength was likely to be originated from the variation in transmembrane proteins–lipid interactions.

1. Introduction

Understanding the mechanical behavior of cells has great implications in tissue engineering and regenerative medicine. Control of cell behavior and/or cell fate can be exercised if exquisite linkages between external stimuli and cell response can be established. To this end, quantitative description of cell behavior is necessary and it entails precise measurement of fundamental mechanical properties. Various experimental methods have been used in studying the mechanics of cells, and apparently, much attention has been focused on cell adhesion as well as elastic and viscoelastic behavior (Van Vliet et al., 2003), but less on the rupture behavior of living cells.

For many materials, synthetic or biological, their (mechanical) strength is unlikely a single number but more appropriately described by a statistical distribution. However, whether the strength of living cells or plasma membrane can be described statistically is a fundamental question that has not been properly addressed. Results of such studies will provide insights into the material structure and useful information on injury mechanics at the cellular level.

In this work, we have studied the rupture behavior of two groups of NIH 3T3 fibroblast cells under tension, using micropipette aspiration. The first group of cells was unstained while the second group was stained with TubulinTracker™ (TT) to observe the local deformation of microtubules (MTs) during aspiration. Results were analyzed by the Weibull model, an established statistical model used to describe the strength distribution of many engineering materials and some biological materials such as dentin (Staninec et al., 2002) and fibrillar collagens (Layton and Sastry, 2004), to test its suitability in representing cell membrane rupture data. In addition, we have quantitatively determined the cleavage strength of transmembrane protein–lipid through random sampling of transmembrane proteins (TMPs) volume fraction in cell membrane.

2. Materials and methods

2.1. NIH 3T3 mouse fibroblasts cell culture

NIH 3T3 mouse fibroblasts were purchased from ATCC (USA), and cultured using Dulbecco's Modified Eagle's Medium (DMEM) supplemented with L-glutamine, 10% fetal bovine serum, and 5% penicillin/streptomycin in a 35 mm Petri dish at 37 °C, 5% CO_2.

2.2. Microtubules fluorescence staining

After reaching 70–80% confluence, the fibroblasts were stained with 250 nM of TT Green reagent (Invitrogen) according to the manufacturer's protocol. The stained cells were harvested and transferred into a black, low-wall Petri Dish (FD3510B-100, World Precision Instruments, Inc.) with a coverslip (0.17 mm thick, 10 mm in diameter) coated with 0.1 mg/ml fibronectin (F4759, Sigma-Aldrich) and 200 μl of Hanks balanced salt solution (Invitrogen) for a 10-min incubation.

* Correspondence to: N1.3-B2-11, 70 Nanyang Drive, Singapore 637457, Singapore. Tel.: +65 67905835; fax: +65 67911761.
E-mail address: askliao@ntu.edu.sg (K. Liao).
[1] Present address: Research Center for Molecular Biology, Institute of Life and Health Engineering, Jinan University, Guangzhou 510632, PR China.

0021-9290/$ - see front matter © 2011 Elsevier Ltd. All rights reserved.
doi:10.1016/j.jbiomech.2011.01.010

This is to allow the stained cells to adhere partially to the coverslip, which enables the formation of distinct MTs and provide sufficient cell thickness for aspiration.

2.3. Micropipette aspiration

The semi-adhered live cells were aspirated at constant pressure ranged from 1 to 10 kPa and 37 °C for up to 5 min. The temperature of the cell was maintained using a heating plate (Heatable Universal Mounting Frame M-H, Carl Zeiss). The entire process was monitored in real time using a 100 × oil immersion lens and a fluorescence microscope equipped with a high-speed camera (AxioCam Hsm, Axiovert 40 MAT, Carl Zeiss). The inner diameter of micropipettes varied from 1.5 to 4 μm. A total of 133 cells were tested, of which 60 were control (without TT) and 73 were TT-stained. Unpaired two-sample (with unequal variance) *t*-test was used to examine whether the mean critical length (i.e., the maximum length of aspirated cell measured from the entrance of micropipette just before it breaks for the first time), calculated at various pressure are significantly different.

3. Results and discussion

3.1. Characteristics of plasma membrane rupture

Rupture may or may not occur as a portion of the cell elongates inside the micropipette under negative pressure. Rupture of the cell begins with thinning of cell membrane at a region close to the cell apex (Fig. 1(a)), followed by tether formation spanning as long as 50 μm in some cells, with a thickness ranges from 0.55 to 0.95 μm. Subsequently, within a few seconds, rupture occurs at the interface between the tether and cell apex, leading to the formation of a separate enclosed membrane. The remaining tether retracts slightly towards the main cell body due to intrinsic cell elasticity (Kasza et al., 2007). The break-off part of the cell was lighter in color as shown in the bright-field images (Fig. 1(a)), indicating that it contained less cytoplasmic contents. This is expected as formation bleb may occur due to the aspiration pressure on the cell surface.

Cell rupture involves essentially the plasma membrane and the encapsulated cytoplasm. Because low or no fluorescence of stained MTs were seen at the cell apex region (Fig. 1(b)), no substantial MTs and other cytoskeleton (CSK) components were believed to be involved at the rupture site. However, trivial amount of MTs may still be present in the extended cell portion in the micropipette, but was not visible. It was observed that the MTs were pulled and straightened in the direction of suction at the micropipette entrance (Fig. 1(b)), forming a region of higher MT density. Intuitively, this is a region with higher stiffness and strength, which agrees with the observations that all ruptures had occurred away from the micropipette entrance.

Three different rupture modes that do not seem to relate to the magnitude of the applied pressure were observed, and are represented by aspiration length versus time plots in Fig. 2. In Mode 1, cells experience a single break during aspiration, reflected by a drop of the aspiration length, after which the aspiration length from the host cell continues to increase. In Mode 2, cells undergo multiple ruptures (5 such breaks are shown in Fig. 2) at the initial stage of the aspiration process (typically within 100 s), followed by an increase in aspiration length. In Mode 3, cells are subjected to multiple ruptures throughout the aspiration process (8 such breaks are seen in Fig. 2). The percentage of cells with aforementioned rupture modes is tabulated in Table 1.

The mechanisms behind the three rupture modes are still unclear. It is likely that nucleation and growth of 'holes' on the membrane due to the tensile stress lead to membrane rupture (Evans et al., 2003; Boucher et al., 2007). Upon the application of aspiration pressure, nucleation of a hole occurs on the surface of membrane. Above a certain critical hole size, the hole grows irreversibly, tearing deeper into the membrane which eventually rupture (Boucher et al., 2007). After each break, the cell becomes

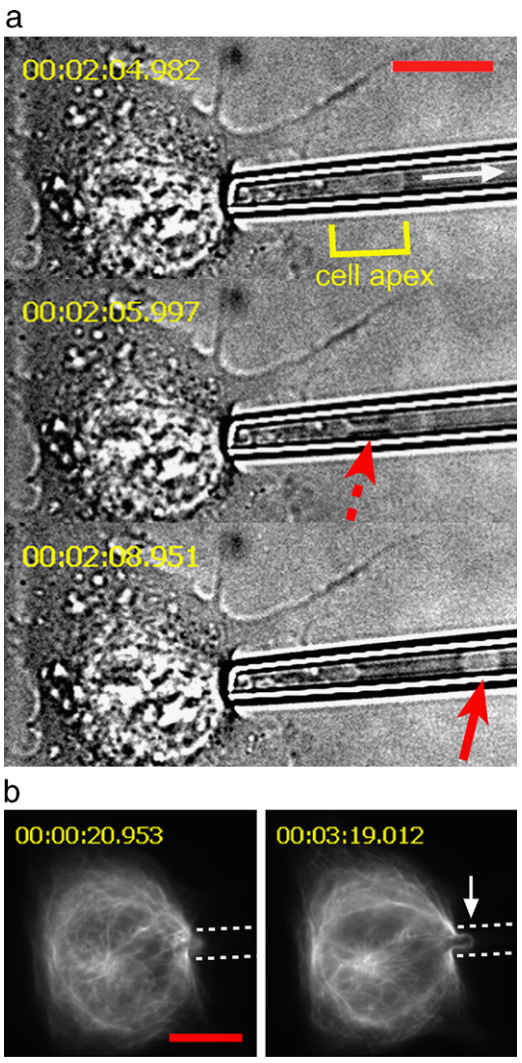

Fig. 1. (a) The time-lapse sequence of apical cell breaking away from its main body at the cell apex region in the direction of suction pressure (white arrow) by forming a tether (dashed red arrow) and an enclosed membrane (red arrow). (b) Straightening of microtubules labeled with TubulinTracker™ (TT) of the same cell shown in (a) at the micropipette entrance (arrow) over aspiration time. It is to be noted that no fluorescence was observed in the region of cytoplasm located further into the micropipette. Scale bars indicate 10 μm. (For interpretation of the references to color in this figure legend, the reader is referred to the web version of this article.)

stiffer (as seen from the decrease of gradient in Fig. 2) due to the loss of the fluid-like cytoplasmic contents, leaving behind the nucleus and intact CSK structure that are more solid-like. In the case of multiple ruptures, the cell experiences a repeated cycle of nucleation and growth of 'holes' after each break. It is speculated that the occurrence of each rupture mode is dependent on the scattering of the size and quantity of holes formed during the sustained stretch. More experiments in the future are required to clarify the proposed mechanism.

For 34% TT-stained and 17% control cells, their nuclei were aspirated together with the cytoplasm due to the close proximity of the nuclei to the micropipette entrance. These cells are referred to as nucleus-aspirated cells (NACs), to be distinguished from non-nucleus aspirated cells (NNACs) described earlier. NACs also experienced all of the three aforementioned rupture modes, except for TT-stained cells where Mode 2 rupture was not seen. A small percentage of cells (8% for both control and TT-stained cells of NNACs and NACs) did not experience any rupture during aspiration. Instead, they exhibited a distinctive viscoelastic

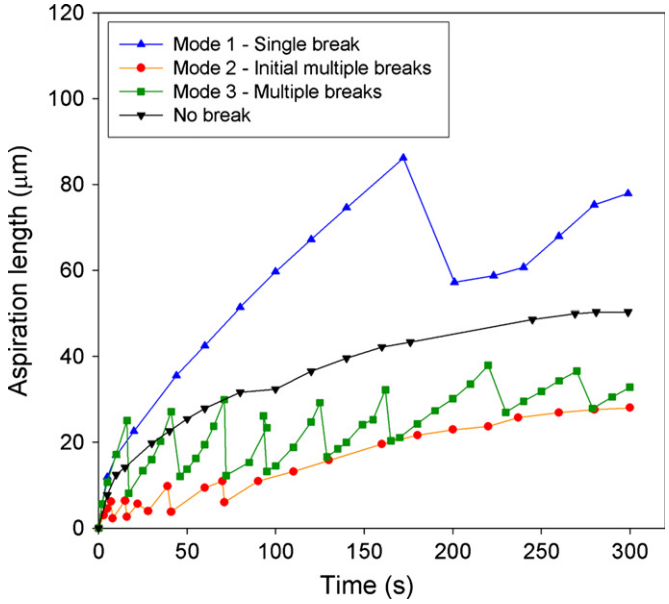

Fig. 2. The various rupture modes and viscoelastic behavior of 3T3 fibroblasts.

Table 1
Percentage of cells in different rupture modes.

Rupture mode	Control (%)		TT-stained (%)	
	NNAC	NAC	NNAC	NAC
1	15	17[a]	3	34[b]
2	10		21	
3	50		34	
No rupture	8[c]		8[c]	

NNAC stands for non-nucleus aspirated cell while NAC is for nucleus-aspirated cell.

[a] All 3 modes are seen.
[b] Only Modes 1 and 3 are seen.
[c] For both NNAC and NAC.

behavior characterized by the steady increase in aspiration length that approaches equilibrium after certain time (Fig. 2), which is similar to result for the aspiration of viscoelastic cellular aggregates (Guevorkian et al., 2010).

3.2. *Effects of microtubules flexibility and contributions of cell nucleus on critical length*

Because of the effect of TT and blockage imposed by the aspirated nucleus, it is believed that the "material" structures of cell in the micropipette are different for the four different groups, i.e., NNACs (TT-stained and control) and NACs (TT-stained and control). TT contains Taxol, a chemical that suppresses and stabilizes the movement of free moving MTs by making them *less* dynamic (Debrabander et al., 1981; Kingston, 2005). As a result, it is anticipated that there were less mobile MT fragments in the aspirated section of TT-stained cells than in the control cells. This is evident from Fig. 1(b) where the TT-stained MTs did not flow deeper into the micropipette together with the aspirated cytoplasm over time. In contrast, the presence of randomly distributed mobile MT fragments in control cells, which was observed as bright fluorescence in the aspirated section of cells with enhanced green fluorescent protein (eGFP) labeled MT (image not shown), may be viewed from the perspective of material science as defects that render the aspirated section of control cells to be more inhomogeneous than the TT-stained cells. As eGFP does not affect the MT dynamics (Ludin and Matus, 1998; Viallet and Vo-Dinh, 2005), eGFP-stained cells are considered to be good representative of our control cells. For NACs, because of blockage by the nucleus at the micropipette entrance, less CSK components were aspirated such that the cell content in the micropipette was more fluidic and homogeneous than those of NNACs. Taken together, the degree of homogeneity for the four different cell groups in descending order is: NACs (TT-stained), NACs (control), NNACs (TT-stained), and NNACs (control). This order is also indicative of the decreasing fluidity of the cell portion in the micropipette.

The critical length of membrane rupture, an indication of "failure strain", is plotted in Fig. 3, against rupture tension. NNACs (TT-stained) are generally having longer critical lengths compared to NNACs (control). There is no strong correlation between critical length and the rupture tension range for both NNACs (control) ($p > 0.1$) and NNACs (TT-stained) ($p > 0.1$). In general, NACs have longer critical lengths compared to NNACs (Fig. 3). The critical length of NACs (control) displays a significant increase of 160% compared to NNACs (control) at the 4–6 mN/m range ($p < 0.05$). NACs (TT-stained) experience a significant jump in critical length by 284% and 161% from the NNACs (TT-stained) at the 2–4 mN/m and 4–6 mN/m range, respectively ($p < 0.05$). There is a significant increase of 331% in the critical length of NACs (TT-stained) as compared to NACs (control) at 2–4 mN/m range ($p < 0.01$). The trend shown in Fig. 3 may be governed statistically due to the scattering of defects (holes) in the membrane and may be represented by Weibull distribution, which will be explored in Section 3.3.

No data on NACs was available within the rupture tension range of 0–2 mN/m as the tension was not sufficient to dislodge the nucleus from its original position. The minimum range of membrane tension required to aspirate the nucleus of NACs (TT-stained) was about 2–4 mN/m higher than that for NACs (control) because the nucleus of NACs (TT-stained) were better secured by the stiffer network of TT-stained MTs. Similar to NNACs, there is no significant correlation between the critical length and the membrane tension applied, for both NACs (control) ($p > 0.1$) and NACs (TT-stained) ($p > 0.1$). The results from critical length measurements seem to support the proposed cell homogeneity discussed earlier: the more fluidic the cell content, the longer the critical length (Table 2).

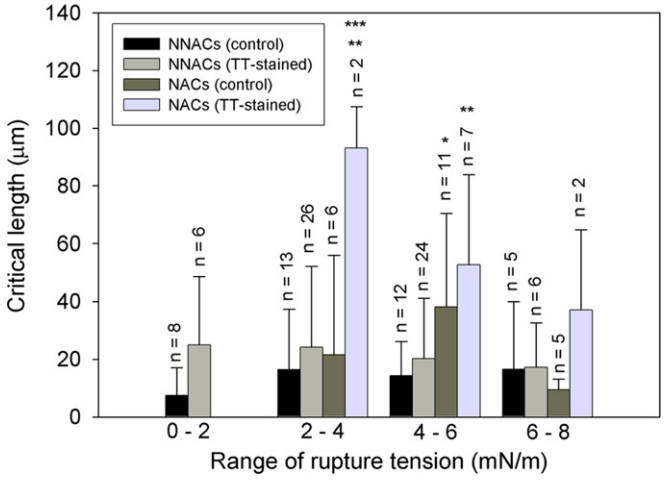

Fig. 3. The comparison of the mean critical length with its respective standard deviation obtained between control and TT-stained 3T3 fibroblasts at various range of membrane rupture tension. $^{*}p < 0.05$ as compared to NNACs (control) at 4–6 mN/m range. $^{**}p < 0.05$ as compared to NNACs (TT-stained) at 2–4 and 4–6 mN/m range, respectively. $^{***}p < 0.01$ as compared to NACs (control) at 2–4 mN/m range.

Table 2
Results of Weibull statistics and critical length.

Cell group	m	τ_o (mN/m)	R^2	τ_{avg} (mN/m)	Critical length
NNACs (control)	1.86	4.40	0.986	3.83 ± 1.94	Lowest
NNACs (TT-stained)	2.68	4.48	0.987	3.98 ± 1.54	Low
NACs (control)	3.85	5.50	0.942	4.98 ± 1.35	High
NACs (TT-stained)	3.23	5.73	0.927	5.12 ± 1.44	Highest

m is the Weibull modulus, τ_o is the characteristic strength, R^2 is the coefficient of correlation, and τ_{avg} is the weighted average membrane strength.

3.3. Statistical analysis of membrane rupture

From the observations of failure modes, it is assumed that the suction in the micropipette is primarily sustained by plasma membrane. The membrane tension (in force/unit length), τ, experienced by the aspirated cell is

$$\tau = \frac{Pr}{2[1-(r/R_s)]} \tag{1}$$

which is derived from the Laplace formula (Kwok and Evans, 1981; Evans et al., 2003) where P is applied suction pressure, r is the inner radius of micropipette and R_s is the radius of cell portion outside the micropipette. τ is calculated for the first break of each cell and taken as the tensile strength of the plasma membrane.

Weibull model is based on weakest link concept where the strength of the material is controlled by the most significant defect, i.e., a material fails when the weakest chain fails (Weibull, 1951). The variations in distribution of strength are due to the random distribution of defects in the material. In our case, defects could be initiated at the TMP-lipid sites and subsequently evolved into holes in the membrane from the sustained tensile stress. To describe the tensile strength distribution of plasma membrane, two-parameter Weibull distribution is used

$$P_f = 1-\exp\left[-\left(\frac{\tau}{\tau_o}\right)^m\right] \tag{2}$$

where P_f is the cumulative density function (cdf) of rupture, τ_o is known as the characteristic strength, and m the Weibull modulus. P_f at a specific applied stress, τ, is calculated by the Median Rank method where $P_f = (i-0.3)/(n+0.4)$. Median Rank method (Johnson, 1951) is a widely used estimate for the cdf of ordered failure data, from $i=1$ to $i=n$ where n is sample size (Dodson, 2006). Here, i is the rank of a specific τ value among all of the strength data in ascending order. τ_o and m can be estimated by linear regression after transforming Eq. (2) into linear form, plotting $\ln[-\ln(1-P_f)]$ against $\ln \tau$ (Fig. 4(a)). Results including the weighted average membrane strength, τ_{avg}, are tabulated in Table 2.

Anderson–Darling (A-D) test, commonly used to perform goodness-of-fit tests on Weibull distributions (Stephens, 1974; Dodson, 2006), was applied to verify whether Weibull distribution is a good fit for the data obtained from each cell group (see Appendix A for calculation method). As shown in Table 3, the test statistic, A^2, for all cell groups are much lower than the critical value, A^2_{crit}, at significant level of 0.05, implying that the tensile strength of cell membrane is adequately described by Weibull model.

τ_o and τ_{avg} for NNACs (control) are lower than NNACs (TT-stained), and the same trend applies for NACs (Table 2). This shows that the rupture strength for control cells, which contain more dynamic MTs, is essentially lower than TT-stained cells. The range of τ_{avg} for each cell group (3.8–5.1 mN/m) corresponds to the region of 2–6 mN/m where the maximum critical length is found (Fig. 3). For NNACs, the fact that the calculated $m<3$ for both control and TT-stained cells suggests that the membrane tensile strength has large scattering (Greek et al., 1997; Kutz, 2002) and the material structure is inhomogeneous. For NACs, the scattering is lesser, reflected by the higher m (>3). This is attributed to the hindrance imposed on CSK flow into the micropipette by the nucleus, leading to a more homogeneous cytoplasm. It is interesting to observe that τ_o and τ_{avg} follow the order of material homogeneity discussed earlier. Overall, the probability of rupture at a specific stress follows essentially the same trend for material homogeneity (Fig. 4(a)).

τ_{avg} calculated from this study is lower than that of phosphatidylcholine (PC) membrane and polyunsaturated PC lipid bilayers, which were found to be 9.4 (Zhelev, 1998) and 5 mN/m (Olbrich et al., 2000), respectively. The difference is believed to be primarily attributed to the structural heterogeneity of the plasma membrane of the living cell where cholesterol (Ikonen, 2008), lipid rafts (Simons and Ikonen, 1997) and TMPs are embedded in the lipid bilayer (Marguet et al., 2006). It has been determined that the presence of peptides in membrane leads to lower rupture tension of lipid vesicles (Boucher et al., 2007). In contrast, the presence of cholesterol (Hsueh et al., 2007) and lipid rafts (Rawicz et al., 2008) increase the membrane resistance to rupture. Therefore, it is clear that the strength of the plasma membrane is determined by the strength of the interaction between lipids and their surrounding components.

3.4. Transmembrane proteins–lipid cleavage strength

Assuming that the cell membrane is a composite material consisting of lipids and TMPs, the strength of the cell membrane (force/unit length), τ_m, can be expressed in a "rule of mixture" type formulation

$$\tau_m = (1-\alpha)\,\tau_{l-l} + \alpha\,\tau_{p-l} \tag{3}$$

where τ_{l-l} is the lipid–lipid cleavage strength, τ_{p-l} is the TMP–lipid cleavage strength, and α is the volume fraction of TMP. Rearranging Eq. (3)

$$\tau_{p-l} = \frac{\tau_m-(1-\alpha)\tau_{l-l}}{\alpha} \tag{4}$$

Substituting $\tau_{avg}=\tau_m=3.83 \pm 1.94$ mN/m (from present study), $\tau_{l-l}=4.9 \pm 1.6$ mN/m (Olbrich et al., 2000) and the widely accepted value of $\alpha=0.5$ (Alberts et al., 2002) into Eq. (4), τ_{p-l} was calculated to be 2.64 ± 0.64 mN/m.

According to Afrin et al. (2003), the average force required to pull membrane proteins out from cell membrane is $\sim$0.5 nN. The line force of pullout, f, is $F/2\pi r$, where F is the pullout force, and r is the radius of the TMP spanning the lipid bilayer. Based on the results of Afrin et al. (2003) and an estimated value of $r=5$ nm, the corresponding TMP–lipid adhesion strength is $\sim$16 mN/m. This value, representing TMP–lipid interaction along the normal of the membrane surface, is six times larger than the estimated τ_{p-l} from the present study. The difference could be attributed to the fact that much larger pulling force is needed to dissociate individual TMPs in the through-the-thickness direction, both from the sea of lipids and the connected, underlying CSK network. In contrast, the TMPs in our study were separated laterally from the lipid membrane at the location of rupture, parallel to direction of aspiration pressure (Fig. 4(b)). The membrane rupture process also involves the dissociation between the lipid–lipid domains along the line of separation. Immediately after the separation of TMPs from the lipids, the surrounding lipids rearrange themselves to prevent the exposure of hydrophobic tails to water and thus, returning the lipids to their energetically favorable state.

3.5. Verification of membrane strength distribution

To explore whether τ_m follows the Weibull distribution because of the randomness of α, a series of τ_m ($n=100$) was

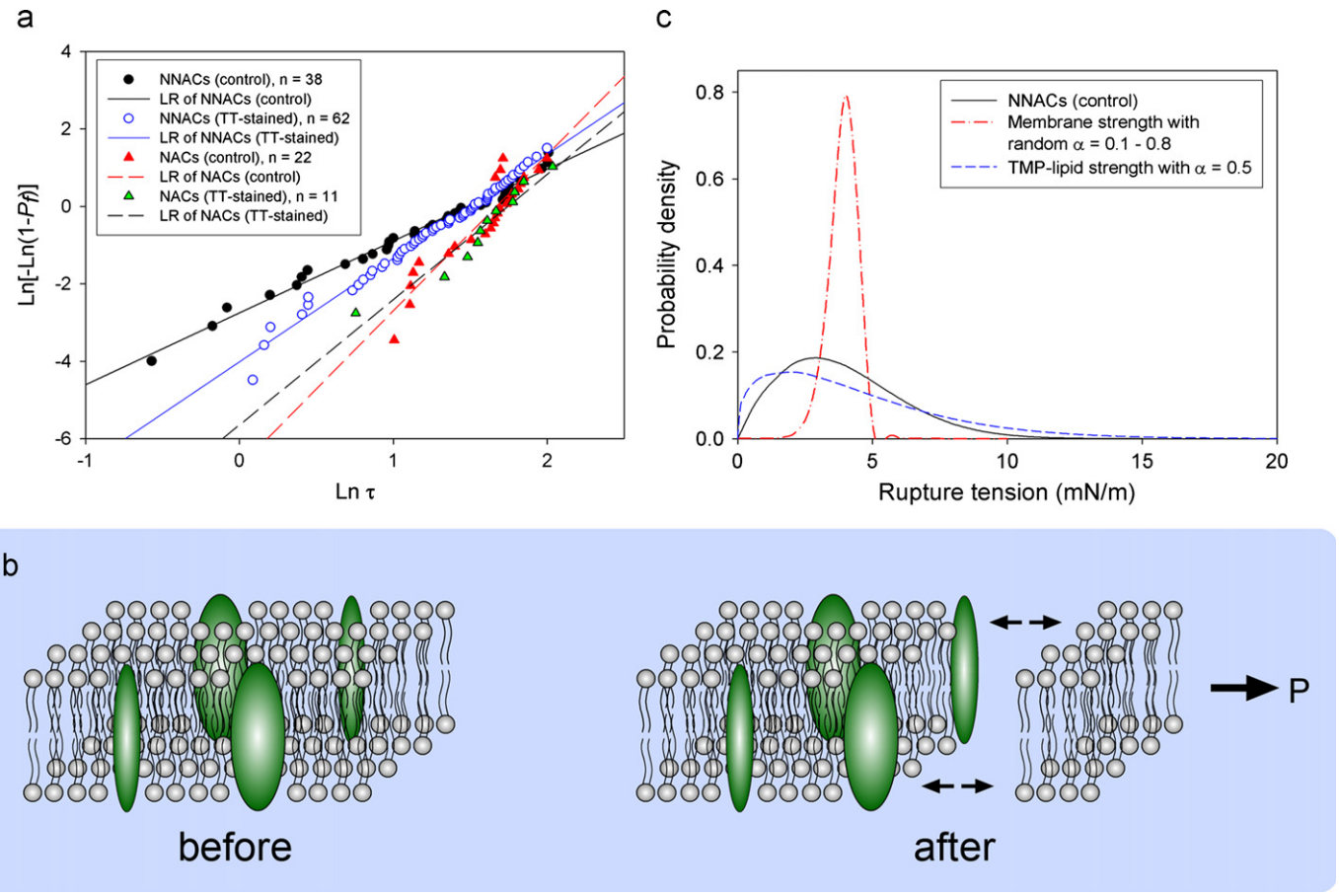

Fig. 4. Weibull analysis for cell membrane and TMP-lipid cleavage strength. (a) Linear plot of Weibull distribution for control and stained cells. LR refers to linear regression line. (b) An illustration of a small section of plasma membrane consisting of lipids (gray) and TMP (green), before and immediately after rupture due to external tensile stress, *P*. (c) A comparison between the Weibull probability density functions of membrane strength calculated from experimental data, random sampling of TMP volume fraction, and TMP-lipid cleavage strength. (For interpretation of the references to color in this figure legend, the reader is referred to the web version of this article.)

Table 3
Results of Anderson–Darling test.

	NNACs (control)	NNACs (TT-stained)	NACs (control)	NACs (TT-stained)
Sample size	38	62	22	11
Calculated value of A^2	0.3459	0.1920	0.3740	0.3833
$A^2_{\text{crit},0.05}$	2.492	2.492	2.492	2.492
Reject H_0 if $A^2 > A^2_{\text{crit}}$	No	No	No	No

A^2 is the test statistic value and $A^2_{\text{crit},0.05}$ is the critical value at a significant level of 0.05.

Table 4
Results of Wilcoxon rank sum test.

Test samples	A vs. B	A vs. C
Calculated value of Z	−0.481	0.700
Reject H_0 if $Z < -1.96$ or $Z > 1.96$ at significant level of 5%	No	No

Sample A is NNACs (control), sample B is the membrane strength at random α=0.1–0.8, and sample C is the TMP–lipid cleavage strength at α=0.5 where α is volume fraction of TMP.

computed using Eq. (3) by randomly assigning α between 0.1 and 0.8, together with the values obtained earlier for τ_{p-l} (~2.64 mN/m) and τ_{l-l} (~5 mN/m). The simulated membrane strength data were then fitted with Weibull distribution based on m=8.89 and τ_o = 4.11 which were obtained from maximum likelihood estimation (MLE) (see Appendix B for the detailed explanation). The result is plotted in Fig. 4(c) using Weibull probability density function, P_d

$$P_d = \frac{m}{\tau_o}\left(\frac{\tau}{\tau_o}\right)^{m-1}\exp\left[-\left(\frac{\tau}{\tau_o}\right)^{m}\right] \quad (5)$$

Also plotted in Fig. 4(c) is the probability density function of NNACs (control). Based on the Wilcoxon rank sum (WRS) test (Wilcoxon, 1945) result in Table 4, there is no significant difference between the strength of NNACs (control) and the simulated data with random α at significant level of 0.05 (see Appendix C for the test method). This means that it is likely that the simulated data were from the same Weibull distribution as the experimental data. However, as seen from Fig. 4(c), the *simulated* Weibull distribution has a much narrower distribution, i.e., lower scattering of membrane strength as its m is ~5 times larger than NNACs (control). Based on this result, it can be concluded that the statistically distributed membrane strength extracted from experimental data is very unlikely to be dominated by the randomness of α.

Instead, we hypothesize that its Weibull characteristics is likely to be originated from the variation in TMP–lipid interactions (Marsh, 2003). To validate this hypothesis, τ_{p-l} was back-calculated using Eq. (4), adapting α=0.5 together with the experimental data of τ_m and τ_{l-l} (~5 mN/m) to obtain the data of TMP–lipid cleavage strengths. The data were then fitted

with Weibull distribution using Eq. (5) with $m=1.35$ and $\tau_o=4.75$, obtained through MLE. Similarly, there is no significant difference between the strength of NNACs (control) and the simulated data of TMP-lipid strength with $\alpha=0.5$ based on WRS test at the significant level of 0.05 (Table 4). Furthermore, as shown in Fig. 4(c), the fitted curve for TMP-lipid cleavage strengths is very similar to the distribution of NNACs (control), demonstrating that the strength of TMP-lipid interactions is the major contributing factor to the Weibull characteristic of membrane strength.

In summary, we have shown that single fibroblasts experience rupture at the cell apex during the aspiration process over a range of membrane tension. Three different types of rupture modes were observed. The tensile strength of the plasma membrane could be described by the Weibull distribution, and it was dependent on the "material" structure of the cell. From simulation, it was inferred that the origin of plasma membrane tensile strength distribution was likely to be dominated by the strength of TMP–lipid interactions.

Conflict of interest

The authors do not have any financial and personal relationships with other people or organizations that could inappropriately influence this work.

Appendix. Supporting information

Supplementary data associated with this article can be found in the online version at doi:10.1016/j.ebiomech.2011.01.010.

References

Afrin, R., Arakawa, H., Osada, T., Ikai, A., 2003. Extraction of membrane proteins from a living cell surface using the atomic force microscope and covalent crosslinkers. Cell Biochemistry and Biophysics 39, 101–117.

Alberts, B., Johnson, A., Lewis, J., Raff, M., Roberts, K., Walter., P., 2002. Molecular biology of the cell. Garland Science, New York.

Boucher, P.A., Joos, B., Zuckermann, M.J., Fournier, L., 2007. Pore formation in a lipid bilayer under a tension ramp: modeling the distribution of rupture tensions. Biophysical Journal 92, 4344–4355.

Debrabander, M., Geuens, G., Nuydens, R., Willebrords, R., Demey, J., 1981. Taxol induces the assembly of free microtubules in living cells and blocks the organizing capacity of the centrosomes and kinetochores. Proceedings of the National Academy of Sciences of the United States of America—Biological Sciences 78, 5608–5612.

Dodson, B., 2006. The Weibull Analysis Handbook. ASQ Quality Press, Milwaukee.

Evans, E., Heinrich, V., Ludwig, F., Rawicz, W., 2003. Dynamic tension spectroscopy and strength of biomembranes. Biophysical Journal 85, 2342–2350.

Greek, S., Ericson, F., Johansson, S., Schweitz, J.-Å., 1997. In situ tensile strength measurement and Weibull analysis of thick film and thin film micromachined polysilicon structures. Thin Solid Films 292, 247–254.

Guevorkian, K., Colbert, M.J., Durth, M., Dufour, S., Brochard-Wyart, F., 2010. Aspiration of biological viscoelastic drops. Physical Review Letters, 104.

Hsueh, Y.W., Chen, M.T., Patty, P.J., Code, C., Cheng, J., Frisken, B.J., Zuckermann, M., Thewalt, J., 2007. Ergosterol in POPC membranes: physical properties and comparison with structurally similar sterols. Biophysical Journal 92, 1606–1615.

Ikonen, E., 2008. Cellular cholesterol trafficking and compartmentalization. Nature Reviews Molecular Cell Biology 9, 125–138.

Johnson, L.G., 1951. The median ranks of sample values in their population with an application to certain fatigue studies. Industrial Mathematics 2, 1–9.

Kasza, K.E., Rowat, A.C., Liu, J.Y., Angelini, T.E., Brangwynne, C.P., Koenderink, G.H., Weitz, D.A., 2007. The cell as a material. Current Opinion in Cell Biology 19, 101.

Kingston, D.G.I., 2005. Chapter 6: Taxol and Its Analog. In: Newman, D.J., Cragg, G.M., Kingston, D.G.I. (Eds.), Anticancer Agents from Natural Products. CRC Press, Florida, pp. 89–122.

Kutz, M., 2002. Handbook of Materials Selection. John Wiley & Sons, New York.

Kwok, R., Evans, E., 1981. Thermoelasticity of large lecithin bilayer vesicles. Biophysical Journal 35, 637–652.

Layton, B.E., Sastry, A.M., 2004. A mechanical model for collagen fibril load sharing in peripheral nerve of diabetic and nondiabetic rats. Journal of Biomechanical Engineering 126, 803–814.

Ludin, B., Matus, A., 1998. GFP illuminates the cytoskeleton. Trends in Cell Biology 8, 72–77.

Marguet, D., Lenne, P.F., Rigneault, H., He, H.T., 2006. Dynamics in the plasma membrane: how to combine fluidity and order. EMBO Journal 25, 3446–3457.

Marsh, D., 2003. Lipid interactions with transmembrane proteins. Cellular and Molecular Life Sciences 60, 1575–1580.

Olbrich, K., Rawicz, W., Needham, D., Evans, E., 2000. Water permeability and mechanical strength of polyunsaturated lipid bilayers. Biophysical Journal 79, 321–327.

Rawicz, W., Smith, B.A., McIntosh, T.J., Simon, S.A., Evans, E., 2008. Elasticity, strength, and water permeability of bilayers that contain raft microdomain-forming lipids. Biophysical Journal 94, 4725–4736.

Simons, K., Ikonen, E., 1997. Functional rafts in cell membranes. Nature 387, 569–572.

Staninec, M., Marshall, G.W., Hilton, J.F., Pashley, D.H., Gansky, S.A., Marshall, S.J., Kinney, J.H., 2002. Ultimate tensile strength of dentin: evidence for a damage mechanics approach to dentin failure. Journal of Biomedical Materials Research 63, 342–345.

Stephens, M.A., 1974. EDF statistics for goodness of fit and some comparisons. Journal of the American Statistical Association 69, 730–737.

Van Vliet, K.J., Bao, G., Suresh, S., 2003. The biomechanics toolbox: experimental approaches for living cells and biomolecules. Acta Materialia 51, 5881–5905.

Viallet, P.M., Vo-Dinh, T., 2005. Chapter 54: Living-Cell Analysis Using Optical Methods. Taylor & Francis Group.

Weibull, W., 1951. A statistical distribution function of wide applicability. Journal of Applied Mechanics—Transactions of the ASME 18, 293–297.

Wilcoxon, F., 1945. Individual comparisons by ranking methods. Biometrics Bulletin 1, 80–83.

Zhelev, D.V., 1998. Material property characteristics for lipid bilayers containing lysolipid. Biophysical Journal 75, 321–330.